

Investigation on the mechanism of damping behavior of magnetorheological elastomers

This article has been downloaded from IOPscience. Please scroll down to see the full text article.

2012 Smart Mater. Struct. 21 125015

(<http://iopscience.iop.org/0964-1726/21/12/125015>)

View [the table of contents for this issue](#), or go to the [journal homepage](#) for more

Download details:

IP Address: 218.104.71.162

The article was downloaded on 17/11/2012 at 01:41

Please note that [terms and conditions apply](#).

Investigation on the mechanism of damping behavior of magnetorheological elastomers

Jie Yang¹, Xinglong Gong¹, Huaxia Deng², Lijun Qin¹ and Shouhu Xuan¹

¹ CAS Key Laboratory of Mechanical Behavior and Design of Materials, Department of Modern Mechanics, University of Science and Technology of China, Hefei 230027, People's Republic of China

² School of Instrument Science and Opto-electronics Engineering, Hefei University of Technology, Hefei 230009, People's Republic of China

E-mail: gongxl@ustc.edu.cn and hxdeng@hfut.edu.cn

Received 13 August 2012, in final form 30 September 2012

Published 16 November 2012

Online at stacks.iop.org/SMS/21/125015

Abstract

Magnetorheological elastomers (MREs) are a group of smart materials which have many applications such as dynamic vibration absorbers, engine mounts, and so on. The damping behavior is important for applications of MREs. However, the mechanism of the damping of MREs has not been investigated thoroughly. In this study, MREs are modeled as special particle reinforced composites with magneto-induced properties and the mechanism of the damping behavior of MREs is investigated theoretically and experimentally. It has been found that there are three types of damping property in MREs: the intrinsic damping, the interface damping and the magneto-mechanical damping. The presented damping model is successfully validated by damping tests on a series of MRE samples. Furthermore, the relationships between the damping properties and formulas of MREs are discussed; this provides guidance for the manufacture of MREs with various damping properties.

(Some figures may appear in colour only in the online journal)

Nomenclature

MRE	Magnetorheological elastomer	S	Area of relative motion
CIP	Carbonyl iron particle	$(\bar{\sigma}_\tau)_i$	The tangential component of τ at S
PRC	Particle reinforced composite	σ_n, σ_τ	Normal, tangential component of stress at S
D_M	Overall damping of MRE	ε_{cr}	Critical strain of relative movement
D_C	Intrinsic damping	σ_0, ε_0	External stress, strain
D_I	Interface damping	f	Friction coefficient between the matrix material and the CIPs
D_M	Magneto-mechanical hysteresis damping	ζ	Stress concentration coefficient σ_n/σ_0
D_m	Intrinsic damping ratio of the matrix material	V_i	Volume of the i th CIP
D_p	Intrinsic damping	K	Discount coefficient
V_m	Volume fraction of the matrix particles	E_c	Storage modulus of the MRE sample
V_p	Volume fraction of the CIPs	$\varphi =$	Proportion of strongly bonded interface
ϕ	Volume fraction of the CIPs	$\varphi(\sigma_0, \varepsilon_0)$	
D_I^s	Strongly bonded interfacial damping	ΔE	Magneto-induced elastic modulus of the MRE in respond to strain ε
D_I^w	Weakly bonded interfacial damping	E_0	Initial elastic modulus of the MRE sample
ν	Poisson ratio of the matrix material	α	$\frac{dE}{d\varepsilon}$
V	Volume of the MRE sample	E_0	Initial elastic modulus of the MRE
d_i	Radius of the i th CIP	μ_0	Permeability of vacuum

μ_1	Relative permeability of the MRE sample
\vec{H}_0	External magnetic intensity
d	Mean diameter of CIP.

1. Introduction

Magnetorheological elastomers (MREs) are a group of smart materials whose properties can be controlled by an external magnetic field [1–4]. MREs are normally manufactured by mixing magnetic micron-sized particles into soft polymer matrix materials. Thus MREs are regarded as a special kind of particle reinforced composite (PRC) [4–6]. Upon curing the matrix material, the magnetic particles in MREs form chain-like or column-like structures [4, 5, 7]. As a result, MREs not only inherit all the merits of traditional PRCs, but also exhibit numerous novel properties such as magnetorheological behavior, magnetostriction and thixotropy [4, 6]. More specifically, the microstructures and stiffness of MREs are adjustable by external stimuli such as magnetic field and strain, and thus enable a rapid response and reversible mechanical properties [1, 4–6, 8]. Recently, MREs have been proposed for various applications, especially in the field of vibration and noise control, such as tunable and adaptive engine mounts, noise insulation devices, vibration isolators, vibration absorbers, artificial muscles, and so on [9–15].

Researchers have been engaged in developing MREs that exhibit controllable stiffness and damping capacity, since these properties are vital in applications of vibration and noise control [4, 6, 16–18]. Deng *et al* [19] developed an adaptive tuned vibration absorber with improved performance by utilizing MREs, Li *et al* [20] reported the usability of a new force sensor based on MREs and Hasheminejad *et al* [12] employed a tunable MRE cored sandwich plate to achieve notable sound insulation characteristics at high frequencies. Thus far, the reports on MREs have mainly concentrated on enhancing the magneto-induced properties, especially the controllable stiffness properties. The damping behavior of MREs, an important parameter for applications, has not been thoroughly studied. Du *et al* [10] pointed out that damping capacity was crucial to the continuous on–off control in their study on an MRE based isolator and Collette *et al* [21] reported that the controllable damping capacity of an MRE based dynamic vibration absorber (DVA) far outweighs that of a traditional DVA. Therefore, it is necessary to comprehensively investigate the damping behavior of MREs. Many researchers have engaged in this study. For instance, Li *et al* [22] employed a MATLAB optimization algorithm to predict the equivalent stiffness and damping, Choi *et al* [23] adopted a higher order sandwich beam theory to investigate the damping property of MREs and Danas *et al* [24] proposed a transversely isotropic energy density function to describe the magneto-induced mechanical behavior. These models have the ability to explain the experimental results well, yet they cannot provide insight into the damping mechanism of MREs. Ivaneyko *et al* developed a linear elasticity model to describe the mechanical behavior of MREs [25] and Chen *et al* [26] presented an interface slip model to describe the damping

mechanism of MREs. However, the magneto-mechanical damping and intrinsic damping were ignored in their study. To accurately predict the damping properties of MREs, the damping behavior of MREs should be systematically studied via both theoretical modeling and experimental examination.

In this study, the mechanism of the damping behavior of MREs is investigated and a theoretical model is developed. The damping of MREs originates from three categories, the intrinsic damping, the interface damping and the magneto-induced damping. MREs are treated as special PRCs with novel magneto-induced properties, and then the corresponding model is developed to reveal the mechanisms of the damping behavior of MREs and characterize the variables that determine the damping capacity. The proposed model is then validated by damping tests on a series of MRE samples. These MRE samples are prepared with different weight contents of ferromagnetic CIPs and tested under a series of strain amplitudes. The experimental results agree well with the theoretical analysis of the three kinds of damping behavior of MREs. In addition, the parameters of the formulas of MREs that affect the damping behavior are also analyzed; this provides guidance for the manufacture of MREs with controllable damping properties.

2. Damping mechanisms of MREs

MREs can be regarded as special particle reinforced composites (PRCs). They not only possess the qualities of traditional PRCs but also exhibit novel magneto-induced properties [2, 4, 5]. Therefore the damping of MREs is classified into the non-magnetic damping and the magnetic damping. It is widely accepted that the damping of a traditional PRC is a combination of several sources [16, 26, 27]: the intrinsic damping of each individual constituent [17], the interface damping between two material phases [28, 29] and the thermal mismatch and dislocation damping caused by the response strain difference between the two components [27, 30]. Since MREs are usually polymer matrix composites, the dissipation energy caused by the thermal mismatch and dislocation damping is negligible. Thus, in general, the non-magnetic damping is thought to be a combination of intrinsic damping and the interface damping. The magnetic damping of an MRE is a parameter that evaluates the magnetic energy dissipation [31, 32]. It includes the eddy current loss, the magneto-mechanical hysteresis loss and the residual magnetism loss. Usually, the magnetic particles used in manufacturing MREs are soft magnetic material so that the residual loss is negligible and can be ignored. In addition, the magnetic domain in each dipole is adjusted to the external vibration and thus dissipated energy. The corresponding energy loss is known as eddy current loss, and it is closely related to the vibration frequency. However, this type of energy loss is negligible when the strain amplitude exceeds 10^{-4} [31]. Therefore, the magnetic damping is mainly determined by magneto-mechanical hysteresis damping. Based on the analysis, the overall damping capacity of MREs is constituted by three types of damping: the intrinsic damping D_C , the

interface damping D_I and the magneto-mechanical damping D_M . The overall damping capacity of an MRE is then expressed as

$$D_{\text{MRE}} = D_C + D_I + D_M, \quad (1)$$

and the details of each term will be discussed in the following sections.

2.1. Intrinsic damping

Since MREs are special particle reinforced composites made from two materials, the rule of mixtures (ROM) [30] is applicable to describe the intrinsic damping of MREs. The overall intrinsic damping capacity of an MRE is determined by the content and the constitutive damping capacity of each individual component, which can be expressed as

$$D_C = \frac{1}{V_m + V_p} (V_m D_m + V_p D_p) = (1 - \phi) D_m + \phi D_p \quad (2)$$

where V_m is the volume fraction of the matrix particles, V_p is the volume fraction of CIPs, D_C denotes the intrinsic damping capacity of the MRE, D_m denotes the damping ratio of the matrix material, D_p represents the intrinsic damping of the CIPs and ϕ is the volume fraction of the CIPs.

The damping capacity of CIPs is far less than the intrinsic damping capacity of the polymer material, and therefore their contribution to the overall damping capacity is negligible for simplicity. Then the overall intrinsic damping capacity of an MRE with CIP content ϕ is rewritten as

$$D_C = (1 - \phi) D_m. \quad (3)$$

From equation (3), the intrinsic damping is proportion to the volume fraction of matrix material, and the damping capacity will decrease when the volume fraction of CIPs increases.

2.2. Interface damping

The condition of the interfaces is significantly important in determining the damping capacity of PRCs [16, 27]. Considering that MREs are special PRCs, the interfacial condition plays an important role in determining the damping of MREs. However, previous research has failed to comprehensively consider the condition of interface bonding [26]. The interfacial bonding can be classified into three categories [16, 33]: ideal interfaces, strongly bonded interfaces and weakly bonded interfaces. The role of ideal interfaces is to transfer the strain and stress between two material phases, yet they do not contribute to the overall damping. For strongly bonded interfaces, the damping is mainly caused by the stress concentration adjacent to the surface of the reinforcing particles. Meanwhile, in the case of weakly bonded interfaces, the damping is mainly caused by the internal friction between the two material phases where the relative motion takes place.

2.2.1. Strongly bonded interface. It has been reported that the interfacial bonding is strong when the content of reinforced particles and the applied external strain amplitude are low [34]. Due to the discrepancy in the properties between the matrix material and the reinforced particles, a special layer adjacent to the surface of the CIP is generated. The property of this special layer is distinct from each individual component. This layer is named as the interphase. The interphase mainly plays the role of transferring stress between the matrix material and the reinforced particles. However, the thickness of the interphase varies from place to place. As a result, the bonding strength changes accordingly, making interfaces with thin interphases easy to be destroyed. In addition, the stress concentration further damages the weaker bonding. Consequently, the damping capacity of strongly bonded interfaces is determined by two factors: the thickness of the interphase and the stress concentration. The interface damping can be described by utilizing the Eshelby inclusion theory [30]. The interface damping caused by strongly bonded interfaces is expressed as follows [29]:

$$D_1^s = \frac{1}{\tau^2} \frac{1 - \nu}{3\pi(2 - \nu)} \frac{1}{V} \sum_{i=1}^n d_i^3 (\bar{\tau}^2)_i \quad (4)$$

where D_1^s denotes the strongly bonded interfacial damping, τ is the applied shear stress, ν is the Poisson ratio of the matrix material, V is the volume of the sample, d_i is the radius of the i th particle and $(\bar{\tau})_i$ is the component of τ in the plane that has relative motion trends. The following assumption is made to simplify the calculation: the CIPs share the same diameter d , the shear stress of each particle is identical, denoted as $\bar{\tau}_i$, and the stress concentration coefficient $\bar{\tau}_i/\tau$ is taken as 1.5, which is the mean value from previous literature. Then the interface damping can be simplified as

$$D_1^s = \frac{4.5(1 - \nu)}{\pi^2(2 - \nu)} \phi \quad (5)$$

where ϕ is the volume fraction of CIPs.

Equation (5) indicates that the damping due to strongly bonded interfaces is related to two variables: the content of CIPs, ϕ , and the Poisson ratio, ν , of the matrix material; the content of CIPs, ϕ , is an important factor in determining the damping in the case of strongly bonded interfaces, and this damping capacity is proportional to ϕ . In addition, the polymer matrix used in MREs is mainly rubber, and the Poisson ratio of different types of rubber changes little, and usually is deemed to be constant (it usually takes a value of 0.48), and therefore the influence of the Poisson ratio, ν , can be ignored.

2.2.2. Weakly bonded interface. Aside from the inherent weakly bonded interfaces, increment of the strain amplitude also helps to turn some strongly bonded interfaces into weakly bonded interfaces. For the case of weakly bonded interfaces, the dissipation energy is mainly caused by internal friction between the matrix and the reinforced particles during deformation. Therefore, the Coulomb law of friction [27] is suitable for calculating the damping due to weakly bonded

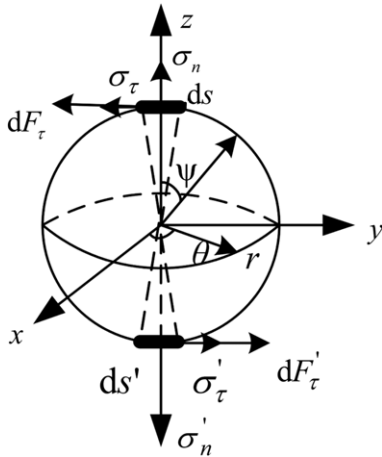


Figure 1. A schematic of the force conditions at the interface where relative movement is likely to occur.

interfaces. In this case, the damping capacity is determined by the friction coefficient between the two constituents and the normal stress at the interface where relative movement is likely to occur. A schematic diagram is shown in figure 1.

As shown in figure 1, the area that has relative movement is denoted as S , ds is the increment of S . When the applied strain amplitude is σ_0 , the normal stress at ds is denoted as σ_n and the corresponding tangential stress is σ_τ . The relative displacement $r(\varepsilon_0 - \varepsilon_{cr})$ occurs when the external stress is sufficient to overcome the resistance generated by friction. Here ε_0 is the corresponding strain amplitude and ε_{cr} is the critical strain of relative movement. Then, according to the Coulomb law of friction, the friction on the area ds is given as

$$d\vec{F}_\tau = f\vec{\sigma}_n ds \times \vec{e}_\tau. \quad (6)$$

Here, f is the friction coefficient between the polymer matrix and the CIPs and \vec{e}_τ is the tangential directional vector.

Since the carbonyl iron particles are treated as ideal balls, and thus the contribution of the tangential stress is symmetric in terms of the whole surface, and the corresponding tangential stresses at the opposite positions of carbonyl iron particles are parallel to each other, the contribution at the area ds is expressed as

$$\begin{aligned} dw &= (\vec{\sigma}_\tau \cdot ds + d\vec{F}_\tau) \cdot d\vec{u} \\ &= (\vec{\sigma}_\tau \cdot ds + f\vec{\sigma}_n ds \times \vec{e}_\tau) \cdot d\vec{u} \end{aligned} \quad (7)$$

where $d\vec{u}$ is the displacement of the carbonyl iron particle.

Similarly, the contribution of the tangential stress contribution at the area ds' is

$$\begin{aligned} dw' &= (\vec{\sigma}'_\tau \times ds' + d\vec{F}'_\tau) \cdot d\vec{u} \\ &= (\vec{\sigma}'_\tau \times ds' + f\vec{\sigma}'_n ds' \times \vec{e}'_\tau) \cdot d\vec{u}. \end{aligned} \quad (8)$$

By comparing dw and dw' , the contribution of the tangential stress is obtained, which is 0. Then the corresponding dissipation energy can be written as

$$dU_{\text{dissipation}} = r(\varepsilon_0 - \varepsilon_{cr})f\sigma_n ds. \quad (9)$$

The dissipation energy in a unit MRE sample is obtained by integrating $dU_{\text{dissipation}}$ over the whole interface, i.e.

$$\begin{aligned} U_{\text{dissipation}} &= \frac{\sum_{i=1}^n \oint r(\varepsilon_0 - \varepsilon_{cr})f\sigma_n ds}{V} \\ &= \frac{3\pi}{4} f\phi\sigma_n(\varepsilon_0 - \varepsilon_{cr}) \end{aligned} \quad (10)$$

where V is the volume of the MRE sample and ϕ is the volume fraction of CIPs. Here the equation $\phi = \frac{1}{V} \sum_{i=1}^n V_i$ is utilized.

In addition, the elastic energy stored in the sample is determined by the following equation:

$$U_{\text{elastic}} = \frac{1}{2}\sigma_0^2/E \quad (11)$$

where σ_0 is the external stress and E is the storage modulus of the MRE sample. Then the damping capacity expressed by the damping factor is derived and expressed as

$$D_1^w = \frac{U_{\text{dissipation}}}{U_{\text{elastic}}} = \frac{3\pi f\phi\sigma_n(\varepsilon_0 - \varepsilon_{cr})}{2\sigma_0^2/E}. \quad (12)$$

Considering that in the case of weakly bonded interfaces ε_{cr} is minimal and far less than ε_0 , equation (12) can be simplified to

$$D_1^w = \frac{3\pi f\phi\sigma_n}{2\sigma_0}. \quad (13)$$

We denote $\zeta = \sigma_n/\sigma_0$ for convenience; it represents the normal stress concentration coefficient at interface S with a relative movement trend. In addition, the stress level at the interface is not always larger than ε_{cr} , and thus relative movement only takes place at part of the interface. Thus it is reasonable to discount the results with a coefficient K ($0 < K < 1$), and then equation (13) is transformed to

$$D_1^w = \frac{3\pi}{2} Kf\phi\zeta. \quad (14)$$

Equation (14) indicates that in the case of a weakly bonded interface, the interface damping is proportional to the CIP content ϕ . Usually, the friction between the CIP and the rubber material is taken as 0.15; ζ increases with the stress level at the interface, and ranges from 1.1 to 1.3 [34]. As a result, the damping due to weakly bonded interfaces increases with the external stress.

The interfaces in MREs are a combination of both weak bonds and strong bonds. Therefore the overall interface damping in an MRE can be written as

$$\begin{aligned} D_1 &= D_1^s + D_1^w = (1 - \varphi) \frac{4.5(1 - \nu)}{\pi(2 - \nu)} \phi \\ &\quad + \varphi \frac{3\pi}{2} Kf\phi\zeta \end{aligned} \quad (15)$$

where $\varphi = \varphi(\sigma_0, \varepsilon_0)$ is the proportion of weakly bonded interface, and it increases with the particle content and the applied strain amplitude. As estimated in [34], it is expressed as

$$\varphi = (1 - \phi)^{1/3} (1 - \varepsilon_0)^{1/3}. \quad (16)$$

Then equation (15) is simplified to

$$\begin{aligned}
 D_I &= [1 - (1 - \phi)^{1/3}(1 - \varepsilon_0)^{1/3}] \frac{4.5(1 - \nu)}{\pi^2(2 - \nu)} \phi \\
 &\quad + (1 - \phi)^{1/3}(1 - \varepsilon_0)^{1/3} \frac{3\pi}{2} Kf\phi\zeta \\
 &= \frac{4.5(1 - \nu)}{\pi^2(2 - \nu)} \phi + \left(\frac{3\pi}{2} Kf\zeta - \frac{4.5(1 - \nu)}{\pi^2(2 - \nu)} \right) \\
 &\quad \times (1 - \phi)^{1/3}(1 - \varepsilon_0)^{1/3} \phi. \quad (17)
 \end{aligned}$$

Equation (17) indicates that the interface damping is closely related to the applied strain amplitude and the content of the reinforcing particles.

2.3. Magneto-mechanical hysteresis damping

Due to the existence of magnetic loss of ferromagnetic reinforced materials, the energy dissipation of ferromagnetic materials is more significant than that in non-magnetic materials [31]. However, the magneto-induced damping in MREs has not been considered in previous models. In this work, the magneto-induced damping is investigated to fully understand the damping properties of MRE materials. The magnetic damping is a parameter that evaluates the capacity of the magnetic loss. The magnetic loss includes three main sources: the eddy current loss, the magneto-mechanical hysteresis loss and the magnetic residual magnetism loss. The eddy current loss is mainly caused by the cyclically alternating magnetization. The alternating magnetic flux density induces macroscopic eddy current loss, and the cyclic changing of magnetic domains leads to microscopic eddy current loss. Both the macro and micro eddy current loss are closely related to the vibration frequency and they are independent of the strain amplitude. However, the corresponding eddy current loss is minimal when the strain amplitude exceeds 10^{-4} or the magnetic particles reach saturated magnetization. Therefore, eddy current losses are ignored in this study. Moreover, the residual magnetism of the CIPs is negligible since they are particles of a soft magnetic material. Consequently, the magneto-elastic damping in MREs is mainly induced by the magneto-mechanical hysteresis. Usually, devices based on MREs work in vibration conditions. Therefore investigation of the magneto-mechanical hysteresis damping is important.

Considering that the cyclic strain amplitude is small, a model based on the Rayleigh loop [31] and Kornetzki's approach [32] is proposed to calculate the magneto-induced dissipation energy, and the relationship between the elastic modulus, E , and the applied strain, ε , can be given by

$$E = E_0 + \alpha\varepsilon \quad (18)$$

where $E = E(\varepsilon)$ is the elastic modulus in correspondence to the external strain ε , E_0 is the initial elastic modulus without applied strain and $\alpha = \frac{dE}{d\varepsilon}$. The corresponding stress is then written as

$$\sigma = E\varepsilon = (E_0 + \alpha\varepsilon)\varepsilon. \quad (19)$$

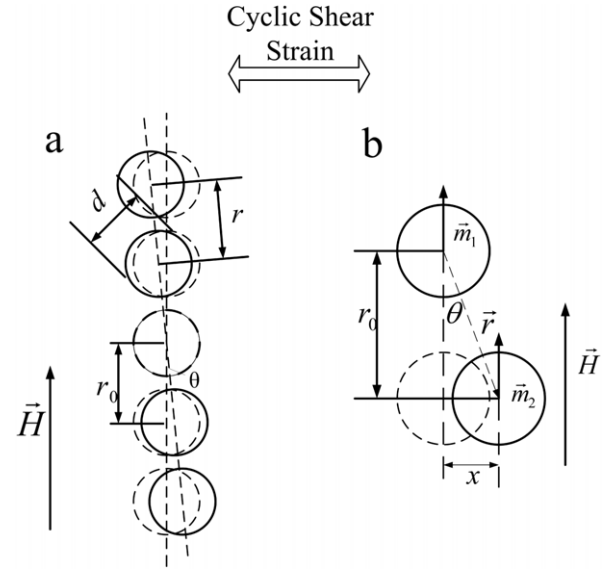


Figure 2. (a) A schematic of the magnetic dipoles in a magnetic field in response to the external strain ε . (b) An enlargement of part of (a); the magnetic moments are \vec{m}_1 and \vec{m}_2 respectively.

The dissipation energy during one load circle is the area of the strain–stress hysteresis loop, which is expressed as

$$\Delta u = \oint \varepsilon d\sigma = \frac{4}{3}\alpha\varepsilon^3. \quad (20)$$

Since the unit elastic energy of an MRE sample during one load circle is expressed as

$$u = \frac{1}{2}E\varepsilon^2, \quad (21)$$

the damping of magneto-mechanical damping is determined by

$$D_M = \frac{1}{2\pi} \frac{\Delta u}{u} = \frac{4}{3\pi} \frac{\alpha\varepsilon}{E}. \quad (22)$$

To determine the damping capacity contributed by magneto-mechanical hysteresis damping, the key issue is to obtain the expression of the elastic modulus E .

It is widely accepted that the magneto-induced property of MREs is caused by the magnetic dipole interactions between adjacent particles in the same chain [24, 35]. Under the driving of an external strain, the particle chains are stretched and deviate from the direction of the magnetic field, as shown in figure 2.

Figure 2 shows a schematic diagram of the deformation of CIPs in a chain under the magnetic intensity \vec{H} . To simplify the computation, the CIPs are assumed to share the same shape (mean diameter d) and central distance r_0 . In addition, the initial center distance between two adjacent particles is also assumed to be identical, denoted by r_0 . As illustrated in figure 2, the CIPs are aligned regularly in a chain, and the length of the chain is assumed to be infinite. Upon loading with a shear strain perpendicular to \vec{H}_0 , the deformed particle chain deviates from the direction of the magnetic field by θ degree, and the center distance is stretched to r . Figure 2(b) illustrates the interaction between two adjacent

CIPs. As mentioned before, the ferromagnetic CIPs are treated as identical, and thus by denoting the magnetic domain of the magnetic dipoles as \vec{m} , the interaction energy of the MRE sample is determined [35] by

$$U = -\frac{3C\phi|\vec{m}|^2(\varepsilon^2 - 2)}{\pi^2\mu_0\mu_1d^3r_0^3(\varepsilon^2 + 1)^{5/2}} \quad (23)$$

where ϕ is the content of CIPs. Then the stress induced by the application of an external magnetic field is obtained by differentiating the total interaction energy with respect to the scalar shear strain, namely

$$\sigma = \frac{dU}{d\varepsilon} = \frac{9C\phi\varepsilon(4 - \varepsilon^2)|\vec{m}|^2}{\pi^2\mu_0\mu_1d^3r_0^3(\varepsilon^2 + 1)^{7/2}}. \quad (24)$$

Similarly, the magneto-induced elastic modulus of an MRE is expressed as

$$\Delta E = \frac{d\sigma}{d\varepsilon} = \frac{9\phi C|\vec{m}|^2(27\varepsilon^2 - 4\varepsilon^4 - 4)}{r_0^3\pi^2d^3\mu_0\mu_1(1 + \varepsilon^2)^{9/2}}. \quad (25)$$

By substituting equation (25) into (22), the damping capacity of an MRE is obtained and simplified as

$$D_M = (12\phi C|\vec{m}|^2\varepsilon^2(20\varepsilon^4 - 205\varepsilon^2 + 90))(r_0^3\pi^3d^3\mu_0\mu_1 \times E_0(1 + \varepsilon^2)^{11/2} + 9\pi\phi C|\vec{m}|^2(27\varepsilon^2 - 4\varepsilon^4 - 4) \times (1 + \varepsilon^2))^{-1}. \quad (26)$$

Equation (26) indicates that the magneto-mechanical hysteresis damping of MREs is determined by the CIP content ϕ and strain amplitude ε . The magneto-mechanical hysteresis damping increases almost linearly with the CIP content ϕ . However, the relationship between the magneto-mechanical hysteresis damping and the strain amplitude is quite complex. The magneto-mechanical hysteresis damping increases nonlinearly with the strain amplitude. In order to simplify the discussion, a term $A(H_0)$ is defined, and $A(H_0) = \mu_0\mu_1\chi[\frac{1}{1-(1/6)C\chi(d/r_0)^3}]$. When the dipoles approach magnetic saturation, $A_s(H_0) = 2.1$ T [36]. Since $m = \frac{1}{6}\pi d^3A(H_0)$, the saturation magnetization is approximated as $m_s = 0.35\pi d^3$. Therefore the magneto-mechanical hysteresis damping is independent of the applied magnetic field when the dipoles become magnetically saturated.

2.4. Overall damping

From the above analysis, the overall damping capacity of an MRE is derived by substituting equations (3), (17) and (26) into equation (1), and thus the overall damping capacity of an MRE is rewritten as

$$D_{MRE} = (1 - \phi)D_m + \frac{4.5(1 - \nu)}{\pi^2(2 - \nu)}\phi + \left(\frac{3\pi}{2}Kf\zeta - \frac{4.5(1 - \nu)}{\pi^2(2 - \nu)}\right) \times (1 - \phi)^{1/3}(1 - \varepsilon_0)^{1/3}\phi + (12\phi C|\vec{m}|^2\varepsilon^2(20\varepsilon^4 - 205\varepsilon^2 + 90))[r_0^3\pi^3d^3 \times \mu_0\mu_1E_0(1 + \varepsilon^2)^{11/2} + 9\pi\phi C|\vec{m}|^2 \times (27\varepsilon^2 - 4\varepsilon^4 - 4)(1 + \varepsilon^2)]^{-1}. \quad (27)$$

Usually, D_m ranges from 0.13 to 0.15, and D_m is taken as 0.14 in this study. The Poisson ratio of rubber materials is usually 0.48, and thus ν is taken as 0.48 here. K denotes the ratio of interfaces that reach the critical value, which is taken as 0.5 in this paper. The friction coefficient between natural rubber and iron ranges from 0.13 to 0.17, and thus f takes the mean value 0.15. C is 1.2 when the particle number is large enough. The initial center distance, r_0 , is usually taken as $1.25d$, and the permeability of rubber, μ_1 , is usually taken as 1; E_0 is taken as 1 MPa. Then equation (27) is transformed and simplified into

$$D_{MRE} = D_m + \left(\frac{29.7}{3200} - D_m\right)\phi + \left(\frac{29.7}{3200} - \frac{9.9\pi}{80}\right) \times (1 - \phi)^{1/3}(1 - \varepsilon_0)^{1/3}\phi + (76.8\phi A^2(H_0)\varepsilon^2 \times (20\varepsilon^4 - 205\varepsilon^2 + 90))[150\pi^2(1 + \varepsilon^2)^{11/2} + 57.6\pi\phi A^2(H_0)(27\varepsilon^2 - 4\varepsilon^4 - 4) \times (1 + \varepsilon^2)]^{-1}. \quad (28)$$

By utilizing the Taylor expansion, $(1 + \varepsilon^2)^{11/2}$ is simplified to $1 + 5.5\varepsilon^2 + 1.875\varepsilon^4 + O(\varepsilon^8)$, then equation (28) is simplified to

$$D_{MRE} = 0.14 + 0.1307\phi + 0.0261(1 - \phi)^{1/3} \times (1 - \varepsilon_0)^{1/3}\phi + (76.8\phi A^2(H_0)\varepsilon^2 \times (20\varepsilon^4 - 205\varepsilon^2 + 90))[150\pi^2(1 + 5.5\varepsilon^2 + 1.875\varepsilon^4 + 14.4375\varepsilon^6) + 57.6\pi\phi A^2(H_0) \times (27\varepsilon^2 - 4\varepsilon^4 - 4)(1 + \varepsilon^2)]^{-1}. \quad (29)$$

As indicated in equation (29), the overall damping capacity is closely related to the volume content of ferromagnetic CIPs, ϕ , and the shear strain amplitude, ε . In addition, the overall damping capacity is independent of the applied magnetic intensity when the magnetic dipoles become saturated. In order to verify these predictions, a series of experiments was conducted, and this will be discussed in section 3.

It is essential to develop a microscopic model to get a comprehensive understanding of the damping behavior of MREs. Most of the reported damping models macroscopically explain the damping behavior of MREs, and few reports have been engaged in investigating the damping behavior of MREs from a microscopic viewpoint. Compared to the microscopic slip model [26], our model take the magneto-induced damping into consideration. Ferromagnetic particles are important components of MREs, thus it is improper to ignore the magneto-induced damping. In addition, all the reinforced particles are assumed to have a relative motion trend in the slip model [26], which is the extreme condition. In our model, we take into the bonding condition into consideration. By referring to the method used in particle reinforced composites, we classify the interfaces into two categories, strongly bonded ones and weakly bonded ones; this is much closer to the real situation. The interfacial bonding condition between the reinforced particles and the matrix has also been considered for modeling the damping property.

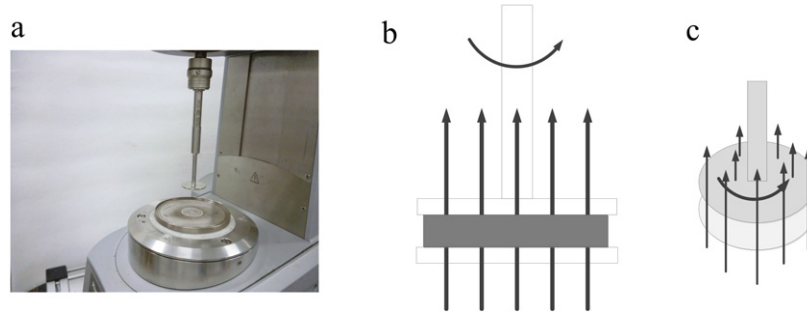


Figure 3. The testing unit of the rheometer and its schematic diagram.

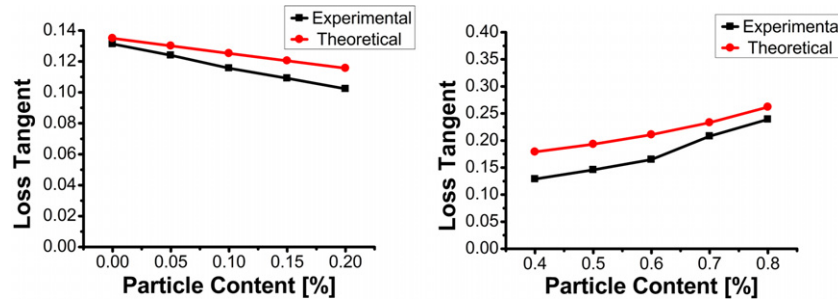


Figure 4. A comparison between the experimental and theoretical results for the relationship between the damping capacity and the CIP content.

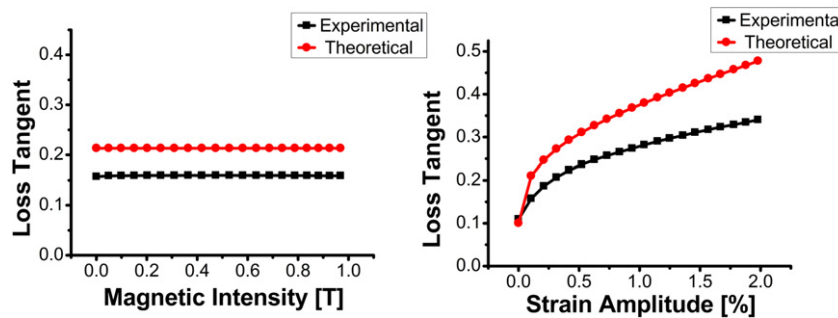


Figure 5. A comparison between the experimental and theoretical results for the relationship between the damping capacity and the strain amplitude.

3. Verification and discussion

To verify the proposed model, a series of MRE samples was manufactured based on our previous reported studies. In this study, two groups of samples with different weight content of CIPs were prepared. In the first group, the weigh contents of CIPs were 0, 5, 10, 15 and 20 wt% respectively, and, for simplicity, the samples were named as MRE-0, MRE-5, MRE-10, MRE-15 and MRE-20 accordingly. In the second group, the particle contents were 40, 50, 60, 70 and 80 wt% separately, and these samples were denoted as MRE-40, MRE-50, MRE-60, MRE-70 and MRE-80 accordingly.

In this study, the damping capacity of the samples was measured by the rotating shear mode of a rheometer (Physica MCR 301, Anton Paar Co.). The testing unit was constituted by two parallel plates, as indicated in figure 3, the bottom one was fixed, and the upper one could generate shear force by rotating. The testing signal was obtained by a sensor connected

to the upper plate. A comparison between the experimental and theoretical results is given in figures 4 and 5.

As shown in figure 4(a), this model predicts that the loss tangent of the experimental result decreases with the particle content when the CIP content is low (below 20 wt%), and the experimental results follow this prediction quite well. Figure 4(b) illustrates the relationship between the damping capacities for samples with high CIP content. In figure 4(b), both the experimental and theoretical damping increase with the CIP content when the CIP content exceeds 40 wt%, and the theoretical results nicely represent the experimental damping behavior in all MRE samples. The experimental damping follows the theoretical damping and changes slightly with the magnetic intensity, as illustrated in figure 5(a). The theoretical damping increases nonlinearly with the strain amplitude and the rate of increase slows down with the strain amplitude in figure 5(b). The experimental results behave consistently with the experimental results.

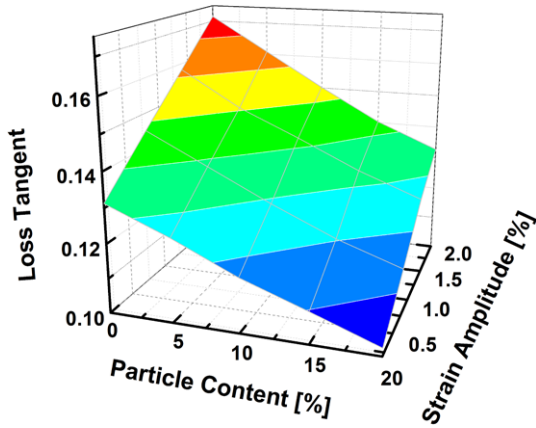


Figure 6. The relationship between damping capacity and strain amplitude. The samples are MRE-0, MRE-5, MRE-10, MRE-15 and MRE-20, and they are tested without a magnetic field.

However, it is worth noting that the theoretical results are larger than the experimental results, and this discrepancy is caused by several reasons. Firstly, when calculating the interface damping, the interfacial bonds are assumed to be either strong or weak, i.e. we denote the proportion of weakly bonded interface as φ , and then the strongly bonded interface is $1 - \varphi$. This assumption overestimates the interfacial damping by assuming that all interfaces contribute to the overall damping. Secondly, it is assumed that the intrinsic damping is caused by the matrix material when calculating the intrinsic damping, while the contribution of the reinforced CIPs is ignored. However, as the CIP content increases, the damping caused by the CIPs (both intrinsic and interfacial damping) cannot be ignored, and thus the theoretical results underestimate the intrinsic damping capacity when the particle content is large. Thirdly, some variables are difficult to obtain, and thus the mean values from previous literatures are used in the calculation. For instance, the damping capacity of natural rubber ranges from 0.116 to 0.233 [34], and in this study it is assumed to be 0.140. Consequently, the discrepancy between the theoretical results and the experimental results is inevitable. In the following sections, each type of damping will be discussed.

3.1. Intrinsic damping

The intrinsic damping is described by equation (5), which indicates that the intrinsic damping is closely related to the intrinsic damping of the matrix material and decreases with the CIP content. However, the other two kinds of damping are also closely related to the particle content, and therefore it is necessary to minimize the interference of the other kinds of damping so as to fully understand the contribution of the intrinsic damping. As analyzed in section 2, the interface damping and the magneto-mechanical damping increase with the strain amplitude and CIP content, and the intrinsic damping will play a dominant role when the CIP content is low. Therefore, a series of MRE samples (MRE-0, MRE-5, MRE-10, MRE-15 and MRE-20) was fabricated so

Table 1. The damping capacities of different samples under different strain amplitudes.

Sample	Strain amplitude			
	0.20%	0.40%	0.60%	0.80%
MRE-0	0.1313	0.1449	0.1581	0.1715
MRE-5	0.1240	0.1360	0.1475	0.1608
MRE-10	0.1156	0.1271	0.1396	0.1502
MRE-15	0.1091	0.1191	0.1312	0.1403
MRE-20	0.1023	0.1128	0.1243	0.1328

as to investigate the intrinsic damping. Without an applied magnetic field, these samples were tested under the same strain amplitudes of 0.2%, 0.8%, 1.4% and 2.0% respectively, in order to eliminate the influence of interface damping and magneto-mechanical damping. The experimental results are shown in figure 6 and table 1.

In figure 6, firstly, the damping capacity (loss tangent $\tan \delta$) of all samples decreases with the CIP content ϕ . As indicated in table 1, the loss tangents, $\tan \delta$, of samples MRE-0, MRE-5, MRE-10, MRE-15 and MRE-20 are 0.1313, 0.1240, 0.1156, 0.1091 and 0.1023 respectively when tested under a strain amplitude of 0.2%. Namely, the damping of all samples decreases with CIP content ϕ . Secondly, although the loss tangent decreases with the CIP content, the damping discrepancy between samples decreases with the strain amplitude. As indicated in table 1, the loss tangents, $\tan \delta$, of the samples MRE-5 and MRE-15 are 0.1240 and 0.1091 respectively at a strain amplitude of 0.2%, and the damping of MRE-5 is 0.0149 larger than that of MRE-15. However, the damping values for MRE-5 and MRE-15 at a strain amplitude of 0.8% are 0.1608 and 0.1403 respectively; the damping of MRE-5 is 0.0205 larger than that of MRE-15. In other words, the damping discrepancies caused by increasing the strain amplitude from 0.2% to 0.8% are 0.0149 and 0.0205 respectively. Thirdly, figure 6 indicates that the $\tan \delta$ decreases with the strain amplitude in each sample. For instance, in table 1, the damping capacities of MRE-10 ($\tan \delta$) are 0.1156, 0.1271, 0.1396 and 0.1502 in response to strain amplitudes of 0.2, 0.4%, 0.6% and 0.8%.

The reasons for this damping behavior are as follows. First, as indicated in equation (5), the loss tangent $\tan \delta$ is determined by the CIP content ϕ , since the intrinsic damping capacity of CIPs is negligible compared with the damping of polymer matrix material. In equation (5), $\tan \delta$ decreases with the CIP content. However, ignoring the intrinsic damping may cause a discrepancy between the theoretical and the experimental results when the CIP content is high. Moreover, the interface damping increases with the CIP content. Thus, intrinsic damping no longer play a predominant role in the overall damping when the CIP content is high, and the contributions of the other two kinds of damping to the overall damping cannot be ignored when the CIP content is high.

3.2. Interface damping

As indicated in section 2.2, the interface damping begins to play a dominant role when the CIP content or the strain

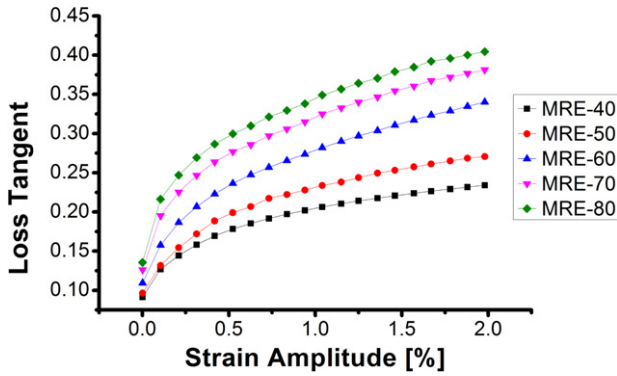


Figure 7. The relationship between damping capacity and strain amplitude. The samples used are MRE-40, MRE-50, MRE-60, MRE-70 and MRE-80, without a magnetic field applied.

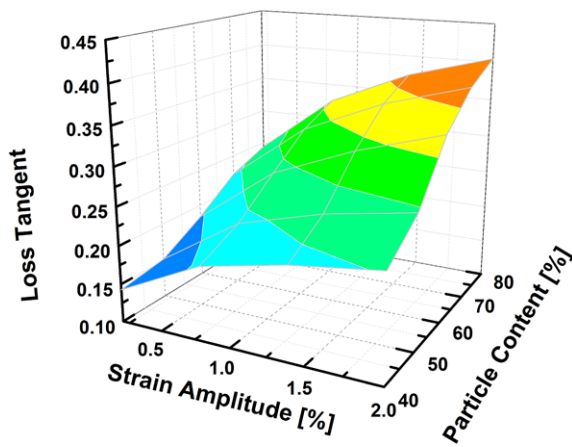


Figure 8. The relationship between damping capacity and strain amplitude. The samples used are MRE-40, MRE-50, MRE-60, MRE-70 and MRE-80, without a magnetic field applied.

amplitude is high. Thus, the damping capacities of a series of MRE samples (MRE-40, MRE-50, MRE-60, MRE-70 and MRE-80) were measured under different strain amplitudes. The CIP content of this group of MRE samples was high so as to decrease the interference of intrinsic damping. The results are shown in figures 7 and 8 and table 2.

As shown in figure 7, firstly, the damping capacities of all the samples increase with the strain amplitude, but the rates of increase slow down with the strain amplitude. Secondly, the damping of all samples increases with CIP content ϕ when tested under the same strain amplitude. In addition, as shown in figure 8, the damping of all samples increases with the CIP content and the strain amplitude. Moreover, as the strain amplitude increases, the damping increment of MRE-80 is larger than that of MRE-40. Table 2 further validates the aforementioned information. On the one hand, $\tan \delta$ increases with ϕ in all samples. For instance, the damping capacities, $\tan \delta$, of samples MRE-40, MRE-50, MRE-60, MRE-70 and MRE-80 are 0.1427, 0.1522, 0.1838, 0.2223 and 0.2440 respectively under a strain amplitude of 0.2%, and the $\tan \delta$ increases with the CIP content. On the other hand, the damping capacity of each sample increases with the strain amplitude. For example, tested under strain

Table 2. The damping capacities of different samples under different strain amplitudes.

Sample	Strain amplitude			
	0.20%	0.80%	1.40%	2.00%
MRE-40	0.1427	0.1953	0.2188	0.2341
MRE-50	0.1522	0.2205	0.2509	0.2706
MRE-60	0.1838	0.2625	0.3065	0.3402
MRE-70	0.2223	0.3027	0.3496	0.3813

amplitudes of 0.2%, 0.8%, 1.4% and 2.0%, the damping capacities of MRE-40 are 0.1427, 0.1953, 0.2188 and 0.2341 respectively, and the damping capacity increases with the strain amplitude. The dependence between $\tan \delta$ and the strain amplitude is applicable to samples with arbitrary CIP content. In addition, although the loss tangent increases with the strain amplitude in all samples, the increment in damping capacity slows down with the strain amplitude. For instance, the loss tangent of MRE-40 increases by 0.0526 when the strain amplitude increases from 0.2% to 0.8% (increment of 0.6%). However, the corresponding increment in loss tangent is only 0.0153 when the strain amplitude increases from 1.4% to 2.0% (increment of 0.6%). The increment in damping capacity decreases with the strain amplitude. c

The reasons for this damping behavior are as follows. Firstly, both the strongly bonded interface damping and the weakly bonded interface damping increase with the CIP content and strain amplitude, and thus the interfacial damping increases with ϕ and ϵ . Secondly, as indicated in equation (16), the proportion of weakly bonded interface increases with CIP content, making the weakly bonded interfacial damping increase with the CIP content. However, the strongly bonded interfacial damping in turn decreases with the CIP content. Consequently, although the interface damping of all samples increases with the strain amplitude, the rate of increase of interfacial damping slows down with the CIP content. This is the same as the relationship between the damping capacity and the strain amplitude, and therefore the damping capacity of all samples increases with the strain amplitude, but the rate of increase slows down with the strain amplitude.

3.3. Magneto-mechanical hysteresis damping

As indicated in equation (26), the damping capacity of MREs is directly related to the strain amplitude and the CIP content. Therefore, the samples MRE-40, MRE-50, MRE-60, MRE-70 and MRE-80 were tested with different magnetic intensities and strain amplitudes. At first, the samples were tested at a strain amplitude of 0.2% with different magnetic intensities. Then the samples were tested at different strain amplitudes without a magnetic field. Figures 9, 10 and table 3 illustrate the corresponding results.

As shown in figure 9(a), the damping capacities of all MREs samples change slightly with the external magnetic intensity. Moreover, when the same strain amplitude is applied, the damping capacity of MREs increases with CIP content ϕ . In figure 9(b), the damping capacity of each sample

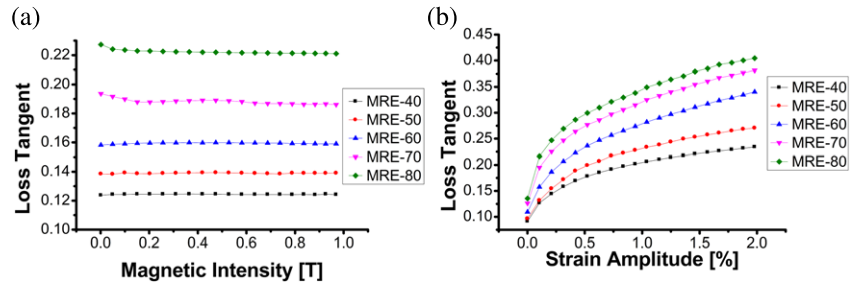


Figure 9. The relationship between the damping capacity and the magnetic field. The samples are MRE-40, MRE-50, MRE-60, MRE-70 and MRE-80. (a) The samples are tested under different magnetic intensities and a strain amplitude of 0.2%. (b) The samples are tested with different strain amplitudes, without a magnetic field.

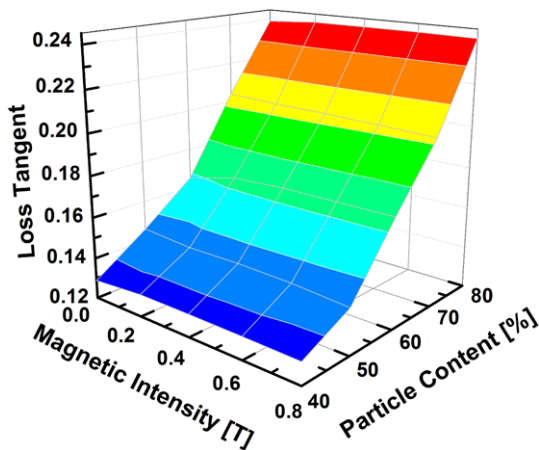


Figure 10. The damping capacities of MREs tested under different magnetic intensities. The strain amplitude is 0.2%.

increases with the strain amplitude, and the rate of increase approximately follows the prediction in equation (26). As illustrated in figure 10, when tested under the same magnetic intensity, the damping capacity of each MRE sample increases with the CIP content. In addition, the damping capacity of the same MRE sample tested under different magnetic intensities changes slightly. Table 3 quantitatively demonstrates the aforementioned conclusions. Firstly, the damping capacity of all MRE samples with different ϕ fluctuates insignificantly with the magnetic intensity. For instance, tested under magnetic intensities of 0, 0.2 T, 0.4 T, 0.6 T and 0.8 T, the corresponding loss tangents of sample MRE-40 are 0.1288, 0.1307, 0.1309, 0.1307 and 0.1305 respectively. The maximum deviation is 1.63%. This can be explained by equation (26): the damping capacity of an MRE is independent of the magnetic intensity when the dipoles reach magnetic saturation. The experimental results further indicate that the contribution of the magneto-mechanical hysteresis damping is much smaller than that of the interfacial damping, and thus the magneto-induced damping does not cause significant changes in the overall damping. Secondly, when tested under the same magnetic intensity, the damping capacities of all MRE samples increase with CIP content. For example, the $\tan \delta$ values for the samples MRE-40, MRE-50, MRE-60, MRE-70 and MRE-80 are 0.1305, 0.1418, 0.1722,

Table 3. The damping capacities of different samples under different magnetic intensities.

Sample	Magnetic intensity				
	0	0.2 T	0.4 T	0.6 T	0.8 T
MRE-40	0.1288	0.1307	0.1309	0.1307	0.1305
MRE-50	0.1459	0.1440	0.1443	0.1436	0.1418
MRE-60	0.1649	0.1710	0.1722	0.1722	0.1722
MRE-70	0.2080	0.2028	0.2024	0.2016	0.2005
MRE-80	0.2391	0.2408	0.2410	0.2411	0.2408

0.2005 and 0.2408 accordingly under an applied magnetic intensity of 0.8 T.

4. Conclusions

In this research, a theoretical model is developed to analyze the damping behavior of MREs. MREs are treated as special particle reinforced composites with novel magneto-induced properties. The overall damping is found to be directly related to the CIP content and strain amplitude. Furthermore, the damping of MREs is constituted by three categories: the intrinsic damping, the interface damping and the magneto-mechanical hysteresis damping. The intrinsic damping plays a dominant role when the CIP content and strain amplitude are low, and thus the overall damping decreases with the content of CIPs at low CIP content. However, the interface damping is predominant at higher strain amplitude or higher CIP content, and thus the overall damping increases with the CIP content and strain amplitude. Moreover, the magneto-mechanical hysteresis damping increases nonlinearly with the strain amplitude. When the dipoles in an MRE reach saturation, the damping is independent of the magnetic field. In addition, a series of experiments was conducted to verify the theoretical results; the theoretical results were found to fairly represent the experimental results, and thus provide guidance for the fabrication of MREs with controllable damping capacity.

Acknowledgments

Financial support from the National Natural Science Foundation of China (Grant Nos 11125210, 11072234, 11102202), the National Basic Research Program of China (973 Program, Grant No. 2012CB937500) and the Specialized

Research Fund for the Doctoral Program of Higher Education of China (Project No. 20093402110010) is gratefully acknowledged.

References

- [1] Ginder J M, Nichols M E, Elie L D and Tardiff J L 1999 Magnetorheological elastomers: properties and applications *Smart Struct. Mater.: Smart Mater. Tech.* **3**675 131–8
- [2] Farshad M and Benine A 2004 Magnetoactive elastomer composites *Polym. Test.* **23** 347–53
- [3] Carlson J D and Jolly M R 2000 MR fluid foam and elastomer devices *Mechatronics* **10** 555–69
- [4] Kallio M, Lindroos T and Aalto S 2006 The elastic and damping properties of magnetorheological elastomers *Appl. Mater. Res. VTT* 110–120
- [5] Filipcsei G, Csetneki I, Szilagyai A and Zrinyi M 2007 Magnetic field-responsive smart polymer composites *Adv. Polym. Sci.* **206** 137–89 (Berlin: Springer)
- [6] Levin M L, Polesskii D É and Prokhorov I V 1997 Some features of the magnetorheological effect *J. Eng. Phys. Thermophys.* **70** 769–73
- [7] Guumlntner D, Borin D Y, Guumlntner S and Odenbach S 2012 X-ray micro-tomographic characterization of field-structured magnetorheological elastomers *Smart Mater. Struct.* **21** 015005
- [8] Wang X J, Gordaninejad F, Calgar M, Liu Y M, Sutrisno J and Fuchs A 2009 Sensing behavior of magnetorheological elastomers *J. Mech. Des.* **131** 091004
- [9] Hoang N, Zhang N and Du H 2011 An adaptive tunable vibration absorber using a new magnetorheological elastomer for vehicular powertrain transient vibration reduction *Smart Mater. Struct.* **20** 015019
- [10] Du H P, Li W H and Zhang N 2011 Semi-active variable stiffness vibration control of vehicle seat suspension using an MR elastomer isolator *Smart Mater. Struct.* **20** 105003
- [11] Mao M, Wereley N M and Browne A L 2010 Adaptive control of a sliding seat using magnetorheological energy absorbers *Proc. ASME Conf. on Smart Materials, Adaptive Structures and Intelligent Systems* vol 2 (New York: American Society of Mechanical Engineers) pp 503–14
- [12] Hasheminejad S M and Shabanimotlagh M 2010 Magnetic-field-dependent sound transmission properties of magnetorheological elastomer-based adaptive panels *Smart Mater. Struct.* **19** 035006
- [13] Boczkowska A and Awietjan S F 2010 Tuning active magnetorheological elastomers for damping applications *Adv. Mater. Forum* **5** 636–637 766–71
- [14] Guo S R, Sun L Y and Chen W W 2011 Control on dynamic response of fluid-driven deployable mechanism by application of magnetorheological elastomeric materials *Adv. Mater. Res.* **183–185** 2313–7
- [15] Boese H, Rabindranath R and Ehrlich J 2012 Soft magnetorheological elastomers as new actuators for valves *J. Intell. Mater. Syst. Struct.* **23** 989–94
- [16] Chandra R, Singh S P and Gupta K 1999 Damping studies in fiber-reinforced composites—a review *Compos. Struct.* **46** 41–51
- [17] Payne A R and Whittaker R E 1971 Low strain dynamic properties of filled rubbers *Rubber Chem. Tech.* **44** 440–78
- [18] Popp K M, Kroeger M, Li W, Zhang X and Kosasih P B 2010 MRE properties under shear and squeeze modes and applications *J. Intell. Mater. Syst. Struct.* **21** 1471–7
- [19] Deng H X and Gong X L 2008 Application of magnetorheological elastomer to vibration absorber *Commun. Nonlinear Sci. Numer. Simul.* **13** 1938–47
- [20] Li W H, Kostidis K, Zhang X Z and Zhou Y 2009 Development of a force sensor working with MR elastomers *2009 IEEE/ASME Int. Conf. on Advanced Intelligent Mechatronics (Singapore)* vols 1–3, pp 233–8
- [21] Collette C, Kroll G, Saive G, Guillemier V and Avraam M 2010 On magnetorheologic elastomers for vibration isolation, damping, and stress reduction in mass-varying structures *J. Intell. Mater. Syst. Struct.* **21** 1463–9
- [22] Li W H, Zhou Y and Tian T F 2010 Viscoelastic properties of MR elastomers under harmonic loading *Rheol. Acta* **49** 733–40
- [23] Choi W J, Xiong Y P and Sheno R A 2010 Vibration characteristics of sandwich beams with steel skins and magnetorheological elastomer cores *Adv. Struct. Eng.* **13** 837–47
- [24] Danas K, Kankanala S V and Triantafyllidis N 2012 Experiments and modeling of iron-particle-filled magnetorheological elastomers *J. Mech. Phys. Solids* **60** 120–38
- [25] Ivaneyko D, Toshchevnikov V P, Saphiannikova M and Heinrich G 2011 Magneto-sensitive elastomers in a homogeneous magnetic field: a regular rectangular lattice model *Macromol. Theory Simul.* **20** 411–24
- [26] Chen L, Gong X L and Li W H 2008 Damping of magnetorheological elastomers *Chin. J. Chem. Phys.* **21** 581–5
- [27] Lavernia E, Perez R and Zhang J 1995 Damping behavior of discontinuously reinforced Al alloy metal–matrix composites *Metall. Mater. Trans. A* **26** 2803–18
- [28] Lavernitiev V I 1997 The mechanism of internal-stress energy damping in the composite material *Metallofiz. Noveish. Tekhnol.* **19** 66–73
- [29] Schoeck G 1969 Internal friction due to precipitation *Phys. Status Solidi* **32** 651–8
- [30] Eshelby J D 1956 The continuum theory of lattice defects *Solid State Phys.* **3** 79–144
- [31] Kuo Y C 1965 *Ferromagnetics* (Peking: People's Education Press) pp 353–355, pp 470–6
- [32] Stoner E C 1936 The internal energy of ferromagnetics *Phil. Trans. R. Soc. A* **235** 165–93
- [33] Lavernia E J, Zhang J and Perez R J 1995 Damping behavior and mechanisms in particulate reinforced metal matrix composites processed using spray atomization and deposition *Key Eng. Mater.* **104–107** 691–728
- [34] Vantomme J 1995 A parametric study of material damping in fibre-reinforced plastics *Composites* **26** 147–53
- [35] Shen Y, Golnaraghi M F and Heppler G R 2004 Experimental research and modeling of magnetorheological elastomers *J. Intell. Mater. Syst. Struct.* **15** 27–35
- [36] Jolly M R, Carlson J D and Munoz B C 1996 A model of the behaviour of magnetorheological materials *Smart Mater. Struct.* **5** 607–14